〈報 文〉

Rate of Sulfur Dioxide Sorption by Alkalized Alumina

Han-Ju Lee

W. R. Grace & Co,
Davison Chemical Division
Clarksville, Maryland, U. S. A.

Abstract

This investigation was carried out for the determination of rate controlling mechanism of SO_2 sorption from a synthetic gas by prototype alkalized alumina.

The theoretical approach was also conducted from the unreacted core shrinking model, while the measurement of rate of SO_2 sorption was gravimetically employed by a torsion balance.

The experimental results pointed that, the unreacted core shrinking model could be applied to SO_2 removal from flue gas by alkalized alumina and its rate was controlled initially by chemical reaction by both chemical reaction and diffusion, in the intermediate stage, and by diffusion at the end.

1. Introduction

Alkalized alumina was originally developed by D. Bienstock and co-workers at the Bureau of Mines, Pittsburgh, Pa. (5) The precipitated alkalized alumina before calcination was identified as a mixture of dawsonite ($NaAlCO_3$ $(OH)_2$) and alumin calcination it becomes sodium aluminate ($Na_2O \cdot xAl_2O_3$) in composition, but has a rather porous structure.

There are several published articles about the alkalized alumina process for removal of SO_2 from flue gas (5, 6, 7). This process will not be discussed further in this paper. However, the alkalized alumina has been recently phased out from the NAPCA program due to some product/process problems.

The rate of SO_2 sorption from a synthetic flue gas by prototype alkalized alumina beads was experimentally studied by the Avco Co. This work was sponsored by the NAPCA of the U. S. Public Health Service and the alkalized alumina was supplied by the Davison Chemical Division of W. R. Grace & Co. In its original report to the NAPCA (1), Avco analyzed the data based on a bulk phase plue pore diffusion model, neglecting the chemical reaction step.

In the present paper, the Avco data was analyzed employing the unreacted-core shrinking model originally developed by Yagi and Kunii for noncatalytic fluid-solid reaction systems (2, 3, 4), and the rate controlling mechanism was determined.

2. Experimental

Although the experimental data were generated by

Avco(1), a brief summary of the experimental work is given below.

The rate of SO_2 sorption was measured gravimetrically employing a torsion balance. A synthetic flue gas was passed around the suspended sample of beads and the weight increase due to SO_2 sorption was determined. The experimental conditions used are summarized in Table 1.

The average particle size was determined by sieving. Carbon dioxide gas was not included in the synthetic flue gas.

The experimental results are summarized in Tables 2-8.

Table 1. Summary of Experimental Conditions

Run No.	Temp. (°C)	Gas Velocity (ft/sec)	Particle Diameter of Alkalized Alumina Beads (in)	Synthetic Flue Gas Composition (Vol. %) SO_2	H_2O	O_2	N_2
S—79	300	7.6	.102	.81	7.2	3.15	88.84
S—80	〃	〃	〃	.96	〃	〃	88.69
S—81	300	〃	.067	.85	〃	〃	88.80
S—82	〃	〃	〃	.92	〃	〃	88.73
S—83	〃	〃	〃	.81	〃	〃	88.84
S—85	300	〃	.086	.96	〃	〃	88.69
S—86	〃	〃	〃	1.02	〃	〃	88.63

Table 2. Run S-79

Sorbent weight—277mg, Saturation weight gain=111mg

Time (min.)	Weight gain (mg)	Time (min.)	Weight gain (mg)	Time (min.)	Weight gain (mg)	Time (min.)	Weight gain (mg)
0	0	6	28.6	22	67.6	54	95.5
.5	3.3	7	32.6	24	70.6	62	98.7
1	6.8	8	35.3	26	73.0	71	101.2
1.5	9.8	10	42.0	29	76.6	80	103.4
2	12.8	12	46.8	32	80.0	90	105.6
2.5	15.0	14	52.0	35	83.0	105	107.3
3	17.3	16	56.0	38	85.5	120	108.4
4	21.5	18	60.1	42	87.3		
5	25.4	20	63.9	48	92.4		

Table 3. Run S—80

Sorbent weight—277mg, Saturation weight gain=111mg

Time (min.)	Weight gain (mg)	Time (min.)	Weight gain (mg)	Time (min.)	Weight gain (min.)	Time (min.)	Weight gain (min.)
0	0	7	29.9	21	61.2	51	91.4
.50	3.9	8	33.6	23	64.8	57	93.8
1.00	7.0	9	36.6	25	67.6	65	97.2
1.50	7.4	10	39.6	28	71.1	75	100.5
2	9.4	11	42.1	31	75.1	85	102.7
3	14.3	13	46.9	34	78.2	100	105.5
4	18.4	15	51.1	37	81.0	115	106.5
5	22.8	17	54.6	41	85.3		
6	27.0	19	57.9	45	87.1		

Table 4. Run S-81

Sorbent weight=270mg, Saturation weight gain=121mg

Time (min.)	Weight gain (mg)	Time (min.)	Weight gain (mg)	Time (min.)	Weight gain (mg)	Time (min.)	Weight gain (mg)
0	0	6	31.4	20	65.2	48	95.6
.5	4.9	7	34.8	23	69.4	53	98.5
1.0	7.5	8	37.8	26	73.2	61	102.4
1.5	9.4	9	43.8	29	77.4	69	105.7
2.0	11.8	10	47.7	32	81.2	79	108.1
3	16.9	12	51.9	35	84.2	94	111.2
4	22.6	14	55.5	39	88.9	109	114.5
5	26.7	17	61.1	43	92.2	124	116.5

Table 5. Run S-82

Sorbent weight=270mg, Saturation weight gain=120mg

Time (min.)	Weight gain (mg)	Time (min.)	Weight gain (mg)	Time (min.)	Weight gain (mg)	Time (min.)	Weight gain (mg)
0	0	4.5	32.6	15.9	64.8	37.0	94.4
.5	7.8	5.5	37.0	17.0	69.0	44.0	99.0
1.0	13.0	6.5	40.5	19.0	73.0	56.0	103.8
1.5	16.8	8.0	45.8	21.0	76.7	68.0	106.9
2.0	20.3	9.5	50.5	24.0	81.3	88.0	110.1
2.5	23.2	11.0	54.5	27.0	85.0	112	112.7
3.5	28.0	13.0	60.0	32.0	90.5		

Table 6. Run S-83

Sorbent weight=238mg, Saturation weight gain=102.7mg

Time (min.)	Weight gain (mg)	Time (min.)	Weight gain (mg)	Time (min.)	Weight gain (mg)	Time (min.)	Weight gain (mg)
0	0	5.5	26.8	20.0	61.5	62	92.0
.5	4.2	7.0	31.6	23	65.7	77	95.3
1.0	8.6	8.5	36.1	27	69.6	92	97.8
1.5	11.4	10.5	41.6	32	74.4	107	99.8
2.0	13.8	12.5	46.4	38	80.3		
3.0	18.1	14.5	51.0	44	85.0		
4.0	21.7	17.0	56.2	52	88.6		

Table 7. Run S-85

Sorbent weight=225mg, Saturation weight gain=140.7mg

Time (min.)	Weight gain (mg)	Time (min.)	Weight gain (mg)	Time (min.)	Weight gain (mg)	Time (min.)	Weight gain (mg)
0	0	2.0	23.8	6	44.4	10	59.2
.5	7.5	3	30.2	7	48.5	11	62.0
1.0	15.0	4	3.55	8	52.4	13	67.6
1.5	18.9	5	40.7	9	55.7	15	72.9

17	77.3	28	96.5	53	116.6	98	131.8
19.5	82.5	32	101.5	63	120.8	123	133.0
22	87.1	37	106.3	73	124.1		
25	92.5	43	109.6	88	128.5		

Table 8. Run S-86

Sorbent weight=225mg, Saturation weight gain=137.8mg

Time (min.)	Weight gain (mg)	Time (min.)	Weight gain (mg)	Time (min.)	Weight gain (mg)	Time (min.)	Weight gain (mg)
0	0	6	45.1	21	84.8	56	117.5
.5	11.9	7	48.8	24	89.3	66	120.0
1.0	17.9	8	52.7	27	93.7	76	124.3
1.5	21.4	9	55.9	30	97.1	86	127.5
2.0	24.8	11	61.8	34	102.1	116	133.6
3	30.7	13	67.3	38	105.6	131	134.9
4	36.4	15	71.9	43	109.8		
5	41.1	19	81.2	49	113.3		

3. Theoretical

The reactions involved in SO_2 removal from flue gas by alkalized alumina, $Na_2O \cdot xAl_2O_3$ in composition, are essentially as follows:

$$SO_2(g)+Na_2O(s)\longrightarrow Na_2SO_3(s) \quad (1)$$

$$SO_2(g)+\frac{1}{2}O_2(g)+Na_2O(s)\longrightarrow Na_2SO_4(s) \quad (2)$$

The first reaction predominates when NO_x is not present in the flue gas. when No_x is present in the flue gas, the second reaction becomes equally important. In any case. the reaction product is a mixture of Na_2SO_3 and Na_2 SO_4 in varying proportions based on the composition of the flue gas. The experimental data analyzed in this work were based on NO_x free synthetic flue gas as given in Table 1, and therefore the major reaction was the first reaction.

The reaction rate was analyzed based on the unreacted-core shrinking model originally developed by Yagi and Kunii (2, 3, 4). In the unreacted-core shrinking model, reaction proceeds at a narrow front which divides the completely reacted zone and the unreacted core. At any time during reaction there exists an unreacted core which shrinks in size as reaction proceeds. In the reaction of SO_2 with alkalized

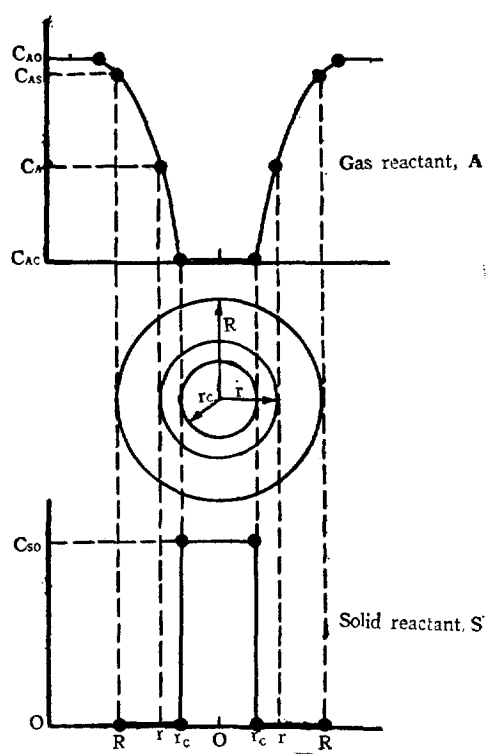

Fig. 1. A Typical Concentration Profile for the Unreacted-Core Shrinking Model

alumina, the product remains in the solid phase and the solid particle size remains essentially constant.

A typical concentration profile for the unreacted-core shrinking model is shown in figure 1.

Taking a mass balance of SO_2 over the product zone, the following differential equation is obtained.

$$\varepsilon\frac{\partial C_A}{\partial t}=D_{eA}\left(\frac{\partial^2 C_A}{\partial r^2}+\frac{2}{r}\cdot\frac{\partial C_A}{\partial r}\right),\quad R>r>r_c \tag{3}$$

The boundary conditions are as follows:

B. C. 1 : At the solid particle surface ($r=R$),

$$D_{eA}\left(\frac{\partial C_A}{\partial r}\right)_R=k_{mA}(C_{Ao}-C_{As}) \tag{4}$$

B. C. 2 : At the unreacted-core front($r=r_c$), assuming an irreversible first order reaction with respect to SO_2,

$$D_{eA}\left(\frac{\partial C_A}{\partial r}\right)_{r_c}=k_s C_{So}C_{Ac} \tag{5}$$

B. C. 3 : Also, at the unreacted-core front,

$$-D_{eA}\left(\frac{\partial C_A}{\partial r}\right)_{r_c}=C_{So}\left(\frac{dr_c}{dt}\right) \tag{6}$$

Eq. (3) can be approximated by assuming pseudo-steady state, or a constant concentration profile of SO_2 in the alkalized alumina bead throughout reaction.

Accuracy of the pseudo-steady state approximation was discussed in detail by C. Y. Wen (4), and is a good approximation for most of the solid-gas reaction systems except for systems with extremely high pressure and very low solid reactant concentration.

In the pseudo-steady state approximation, it assumes

$$\varepsilon\frac{\partial C_A}{\partial t}=0 \tag{7}$$

and Eq. (3) is simplified to give

$$D_{eA}\left(\frac{\partial^2 C_A}{\partial r^2}+\frac{2}{r}\frac{\partial C_A}{\partial r}\right)=0,\quad R>r>r_c \tag{8}$$

Eq. (8) can be solved readily with the boundary conditions given in Eqs. (4) and (5), to give the following concentration profile.

$$\frac{C_A}{C_{Ao}}=\frac{\left(1+\frac{D_{eA}}{k_s C_{So}r_c}\right)\frac{1}{r_c}-\frac{1}{r}}{\left(1+\frac{D_{eA}}{k_s C_{So}r_c}\right)\frac{1}{r_c}-\left(1-\frac{D_{eA}}{k_{mA}R}\right)\frac{1}{R}} \tag{9}$$

Substituting Eq. (9) into Eq. (6), the third boundary condition, the following equation is obtained,

$$t=\frac{RC_{So}}{C_{Ao}}\left[\frac{1}{3}\left(\frac{1}{k_{mA}}-\frac{R}{D_{eA}}\right)\left(1-\frac{r_c^3}{R^3}\right)+\frac{1}{k_s C_{So}}\left(1-\frac{r_c}{R}\right)+\frac{R}{2D_{eA}}\left(1-\frac{r_c^2}{R^2}\right)\right] \tag{10}$$

Eq. (10) gives the reaction time required for an alkalized alumina bead to reduce the unreated core from R to r_c

The conversion, X, can be expressed by the following equation.

$$X=\frac{\left(\frac{4}{3}\right)\pi R^3-\left(\frac{4}{3}\right)\pi r_c^3}{\left(\frac{4}{3}\right)\pi R^3}=1-\left(\frac{r_c}{R}\right)^3 \tag{11}$$

In terms of conversion, X, Eq. (10) becomes,

$$t=\frac{RC_{So}}{C_{Ao}}\left\{\frac{1}{3}\left(\frac{1}{k_{mA}}-\frac{R}{D_{eA}}\right)X+\frac{1}{k_s C_{So}}\left[1-(1-X)^{\frac{1}{3}}\right]+\frac{R}{2D_{eA}}\left[1-(1-X)^{\frac{2}{3}}\right]\right\} \tag{12}$$

At complete conversion time τ, $X=1$, then

$$\tau=\frac{RC_{So}}{C_{Ao}}\left[\frac{1}{3k_{mA}}+\frac{1}{k_s C_{So}}+\frac{R}{6D_e A}\right]$$

$$=\text{a constant} \tag{13}$$

When the gas film resistance controls, $k_{mA}\ll k_s$, D_{eA}, and Eq. (12) becomes

$$t=\left(\frac{RC_{So}}{3k_{mA}C_{Ao}}\right)X \tag{14}$$

$$\text{or}\quad \frac{t}{\tau}=X \tag{14a}$$

When the diffusion through solid phase product layer controls, $D_{eA}\ll k_{mA}$, k_s, and Eq. (12) becomes

$$t=\frac{R^2 C_{So}}{6D_{eA}C_{Ao}}\left[1-3(1-X)^{\frac{2}{3}}+2(1-X)\right] \tag{15}$$

$$\text{or}\quad \frac{t}{\tau}=1-3(1-X)^{\frac{2}{3}}+2(1-X) \tag{15a}$$

When the chemical reaction controls, $k_s\ll k_{mA}$, D_{eA}, and Eq. (12) becomes

$$t=\frac{R}{k_s C_{Ao}}\left[1-(1-X)^{\frac{1}{3}}\right] \tag{16}$$

$$\text{or}\quad \frac{t}{\tau}=1-(1-X)^{\frac{1}{3}} \tag{16a}$$

Eqs. -(14)-(16a) can be used in analyzing experimental data to determine the rate-controlling step.

If t/τ is plotted against $1-(1-X)^{\frac{1}{3}}$ on a log-log scale, Eqs. (14a), (15a) and (16a) give the three different curves shown in Figure 2.

The slope of the plot for the product layer (solid phase) diffusion controlling mechanism at a low conversion level is close to two. Whereas the slopes for film diffusion controlling and chemical reaction controlling mechanisms at low conversion levels are both one.

Apparently the log-log plot of t/τ vs. $1-(1-X)^{\frac{1}{3}}$ alone will not determine clearly between film diffusion.

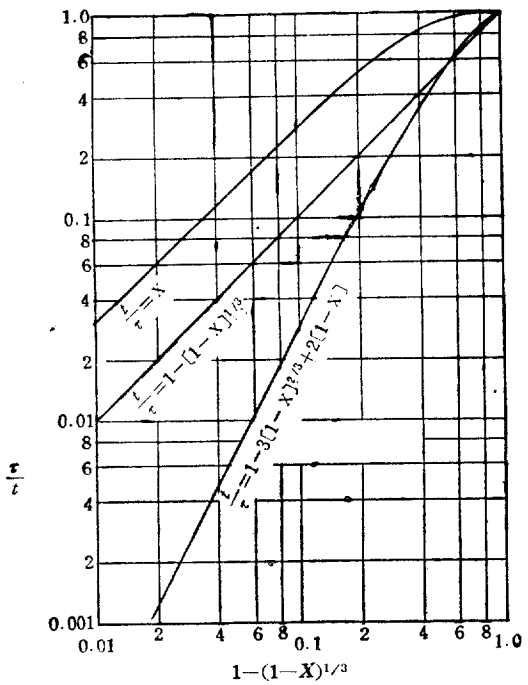

Fig. 2. Characteristic Curves for Rate Determining Steps

controlling and chemical reaction controlling mechanisms, especially at an early stage of reaction.

Fortunately, however, a plot of $(1-X)^{\frac{1}{3}}$ vs. t/τ on the ordinary scale will clearly distinguish the two mechanisms as shown in Figure 3.

In this plot, the chemical reaction controlling mechanism shows a straight line with a negative slope of one, whereas the plot for the film diffusion controlling mechanism is a curve with an initial slope of—1/3.

4. Analysis of the Experimental Data and Discussion

The experimental bata obtained dy Avco were analyzed employing the method described in the previous

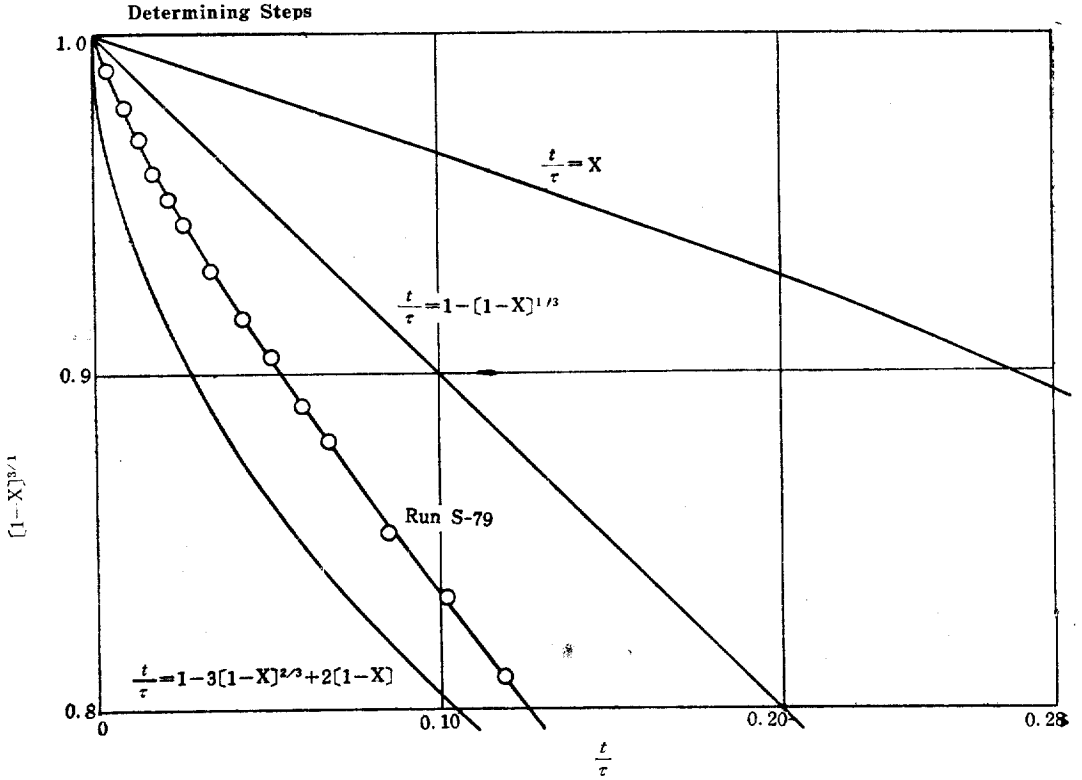

Fig. 3. Characteristic Curves for Rate Determining Steps for Low Conversion Level

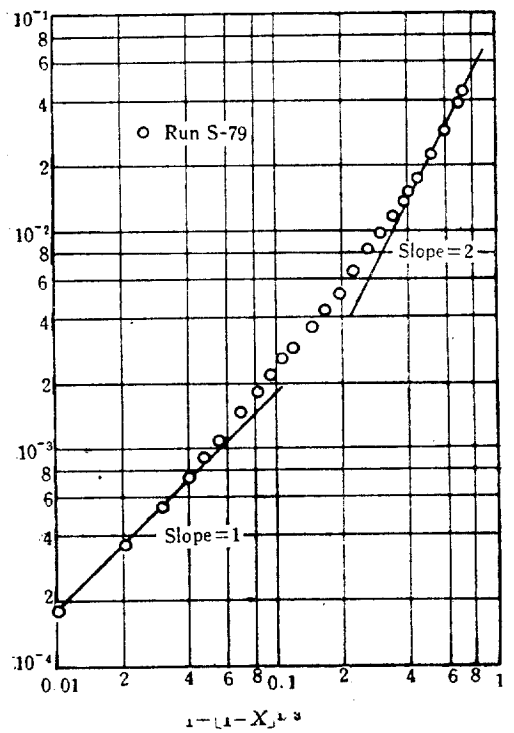

Fig. 4. Analysis of Rate Controlling Mechanism

section.

The rate controlling step was determined first by plotting $C_{Ao}t$ vs. $1-(1-X)^{\frac{1}{3}}$ on a log-log scale. The plot of experimantal data from Run S-79 is shown in Figure 4. $C_{Ao}t$ was used instead of t/τ for convenience here. However, $C_{Ao}t$ is equivalent to (t/τ) times a constant and does not change the slope on a log-log plot.

As clearly shown in Figure 4, the slope at the beginning of the reaction is one. However, as the reaction approaches completion, the slope approaches two.

This analysis indicates that the rate controlling step at the beginning of reaction is either gas-film diffusion controlling or chemical reaction controlling, because both mechanisms have a slope of one at low conversion level. As the reaction approaches completion, however, the product layer (solid-phase) diffusion becomes controlling.

The rate controlling step at the beginning of reaction was further analyzed by plotting $(1-X)^{\frac{1}{3}}$ vs.

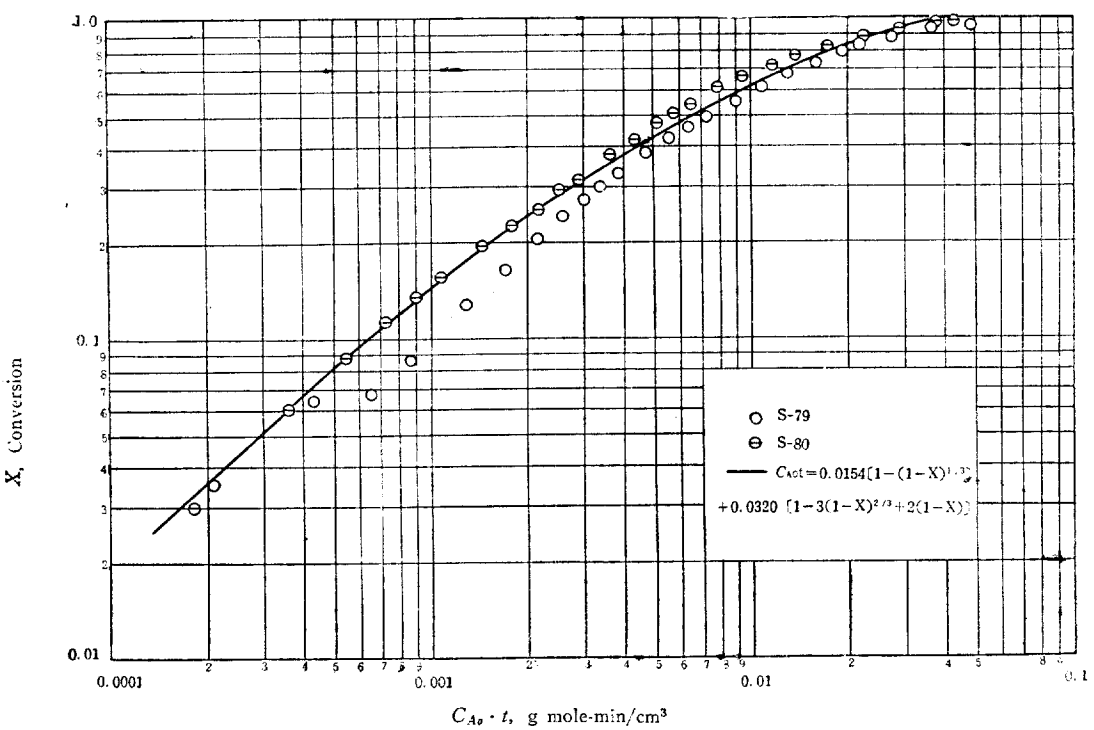

$C_{Ao} \cdot t$, g mole-min/cm³

Fig. 5. Comparison of Experimental Data and Theoretical Solution (R=0.12954 cm)

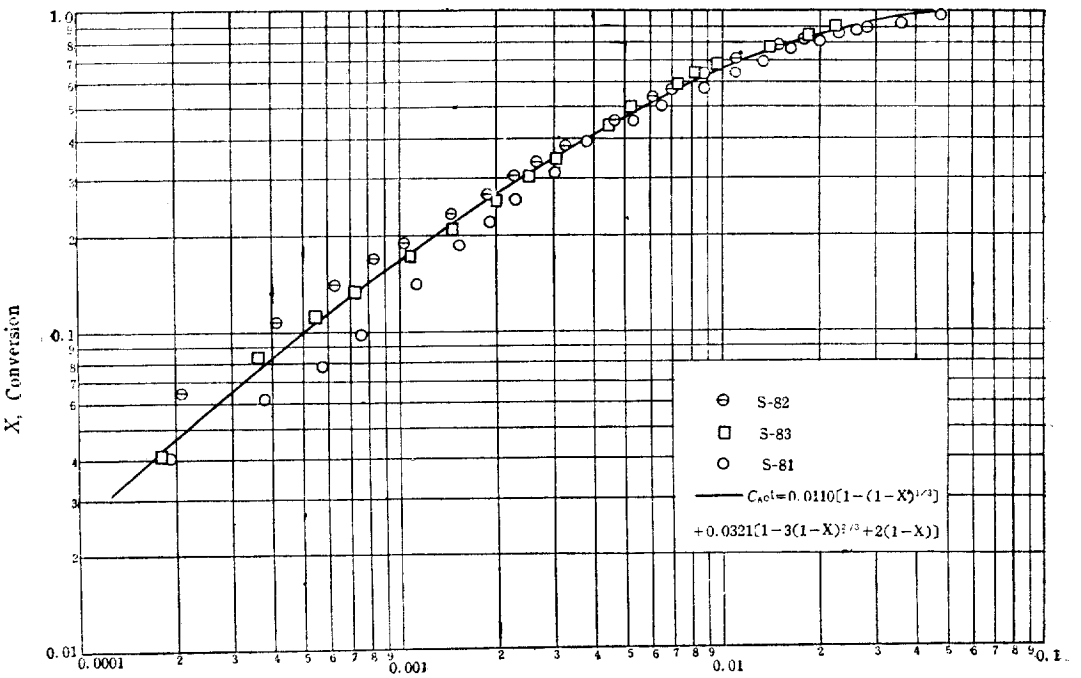

Fig. 6. Comparison of Experimental Data and Theoretical Solution (R=0.10922cm)

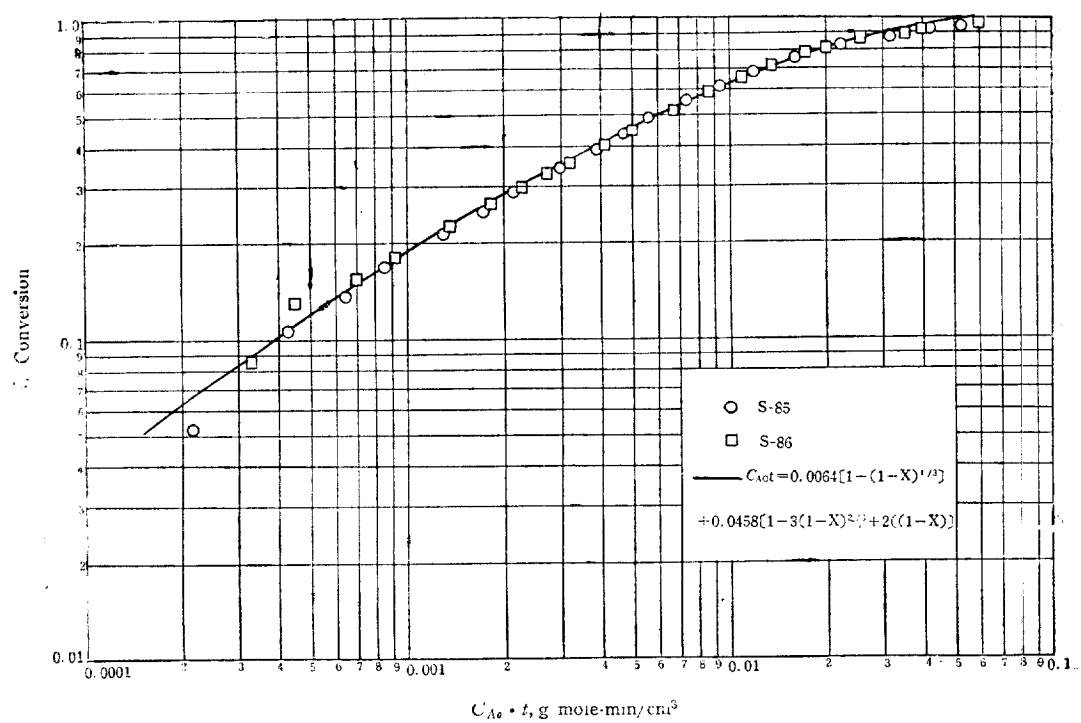

Fig. 7. Comparison of Experimental Data and Theoretical Solution (R=0.08509cm)

t/τ as shown in Figure 3. The experimental data (Run S-79) in Figure 3 definitely indicate the controlling mechanism even at low conversion is either chemical reaction controlling or product layer diffusion controlling or both, definitely not gas-film diffusion controlling.

Summarizing the above analysis, the rate of SO_2 sorption is controlled by

a) chemical reaction at the very early stage,

b) then predominantly by product-layer diffusion at the end

c) and by both chemical reaction and product-layer diffusion in between.

Since the gas-film diffusion was eliminated from the rate controlling steps, the rate equation, Eqs. (10) and (12), can be simplified now to give.

$$C_{A0}t=\frac{R^2 C_{S0}}{6D_{eA}}\left[1-3\left(\frac{r_c}{R}\right)^2+2\left(\frac{r_c}{R}\right)^3\right]+\frac{R}{k_s}\left[1-\frac{r_c}{R}\right] \qquad (17)$$

or

$$C_{A0}t=\frac{R^2 C_{S0}}{6D_{eA}}\left[1-3(1-X)^{\frac{2}{3}}+2(1-X)\right]+\frac{R}{k_S}\left[1-(1-X)^{\frac{1}{3}}\right] \qquad (17a)$$

The constant terms in the above equations, $R^2C_{S0}/6D_{eA}$ and R/k_s, can be calculated from the experimental data. Also, the effective diffusivity in the product layer, D_{eA}, and the reaction rate constant, k_s, can be readily calculated from these constant terms.

The three sets of experimental data in Table 1 were based on three different particle sizes of Alkalized Alumina. The constant terms in Eq. (17a) were computed employing a non-linear regression method based on 0.5 % error for each set of experimental data. Then, the effective diffusivity in the product layer and the reaction rate constant were calculated from these constant terms. The results are summarized in Table 9.

Also, each set of experimental data was compared with the corresponding theoretical solution by plotting X, conversion, vs. $C_{A0}t$ on a log-log scale as shown in Figures 5, 6 and 7. The experimental data match rather well with the theoretical slution.

The effective diffusivity in the product layer and the reaction rate constant were plotted against particle radius in Figure 8.

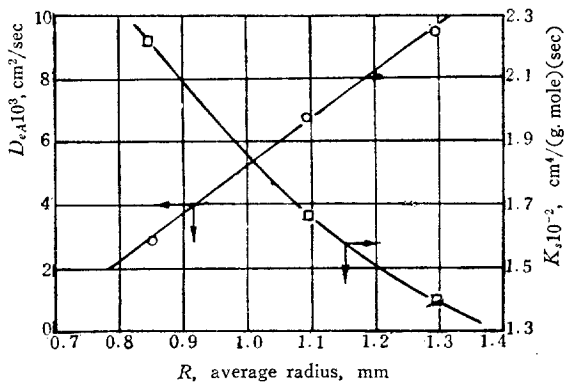

Fig. 8. Effect of Particle Size on D_{eA} and k_s

The effective diffusivity in the product layer increases as the particle size increases, whereas the reaction rate constant decreases as the particle size increases. This effect of particle size on both the effective diffusivity and the reaction rate constant cannot be

Table 9. Computed Constants

Run No.	Particle Radius, R (cm)	$\frac{R^2C_{S0}}{6R_{eA}}$	$\frac{R}{k_s}$	Standard Error in $C_{A0}t$ at 0.5% Error	$D_{eA}X10^3$ cm²/min.	k_sX10^{-2} cm⁴/(g mole) (min.)
S-79	0.12954	0.0320	0.0154	1.2534×10^{-4}	9.315	1.406
S-80						
S-85	0.10622	0.0321	0.0110	1.7088×10^{-4}	6.605	1.653
S-86						
S-81						
S-82	0.08509	0.0458	0.0640	8.7061×10^{-5}	2.808	2.217
S-83						

explanied clearly. However, the following factors may contribute to the unusual effects:

a) Nonhomogeneity of the Alkalized Alumina sample between different particle sizes in chemical composition and pore size distribution.

b) Difficulty connected with obtaining the true representative particle size.

5. Conclusions

1) The unreacted-core-shrinking model can be satisfactorily applied to SO_2 removal from flue gas by Alkalized Alumina.

2) The rate of SO_2 sorption by Alkalized Alumina is controlled

a) initially by the chemical reaction step,

b) by both chemical reaction and diffusion through the product layer in the intermediate stage, and

c) by diffusion through the product layer at the end.

3) The particle size of the prototype Alkalized Alumina beads affects both reaction rate constant and effective diffusivity in the product layer.

Acknowledgement

The author gratefully acknowledges the NAPCA of the Public Health Service and the Davison Chemical Division of W. R. Grace & Co. for permission to publish this paper. The author also acknowledges the Avco Corp. for supplying the experimental data which were obtained with the support of the NAPCA.

Literature

1. Avco, "*Removal of* SO_2 *from Flue Gas*", Final Report PH-86-67-51, Nov. 1, 1967.

2. Yagi, S. and Kunii, D., "*Fifth Symposium (International) on Combustion*", Reinhold, New York, 1955, p. 231.

3. Levenspiel, O., "*Chemical Reaction Engineering*" Wiley, New York, 1962, p. 338.

4. Wen, C. Y., *I. E. C.*, Vol. **60**, No. 9, 1968, p. 34.

5. Bienstock, D., Field, J. H., and Myers, J. G., *Trans, A. S. M. E., J. of Eng. for Power*, **86**, No. 3, 1964, p. 353.

6. Katell, S., *C. E. P.*, **62**, No. 10, 1966, p. 67

7. Cortelyou, C. G., *C. E. P.*, **65**, No. 9, 1969, p. 69.

Nomenclature

C_A : concentration of gas reactant (SO_2), mole/L^3.

C_{Ao} : concentration of gas reactant (SO_2) in bulk phase, mole/L^3.

C_{As} : concentration of gas reactant (SO_2) at external surface of the particle, mole/L^3.

C_{Ac} : concentration of gas reactant (SO_2) in unreacted-core mole/L^3.

C_S : concentration of solid reactant (Na_2O), mole/L^3.

C_{So} : initial concentration of solid reactant (Na_2O) in the particle, or concentration of solid reactant in unreacted-core of the particle, mole/L^3.

D_{eA} : effective diffusivity of gas reactant (SO_2) in product layer, L^2/θ.

k_{mA} : gas film mass transfer coefficient for gas reactant (SO_2), L/θ.

k_s : reaction rate constant based on unit surface area, L^4/(mole) (θ).

R : particle radius, L.

r : distance from the center of spherical particle, L.

r_c : distance from the center of spherical particle to unreacted-core surface, L.

t : time, θ.

X : conversion

ε : particle void fraction.

τ : time for complete conversion